Original Article | **Open Access**

Extracellular Vesicles and Circulating Nucleic Acids

Xu et al. Extracell Vesicles Circ Nucleic Acids. 2026;7:2089-107 **DOI:**10.20517/evcna.2026.220

Purified plasma vesicles modulate inflammation and mineralisation

Tian Xu[1], Dalila Iannotta[2], Zhengming Tang[1], Pingping Han[1], Nigel Johnson[1], Sašo Ivanovski[1], Joy Wolfram[2,3,4], Yinghong Zhou[1]

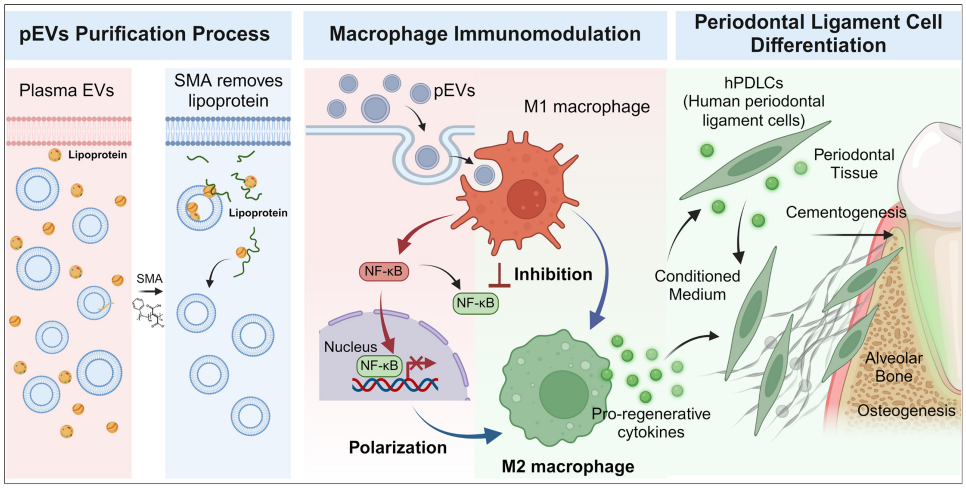
Keywords:
Extracellular vesicles, plasma, lipoprotein, immunomodulation, mineralisation

Citation: Xu T, Iannotta D, Tang Z, Han P, Johnson N, Ivanovski S, Wolfram J, Zhou Y. Purified plasma vesicles modulate inflammation and mineralisation. *Extracell Vesicles Circ Nucleic Acids.* 2026;7:2089-107. https://dx.doi.org/10.20517/evcna.2026.220

Received: 11 Sep 2026
Revised: 29 Oct 2026
Accepted: 30 Oct 2026
Published: 18 Nov 2026

Academic Editors:
Yoke Peng Loh, Lexie Shannon Holliday
Copy Editor:
Ting-Ting Hu
Production Editor:
Ting-Ting Hu

Check for updates



Abstract

Aim: Plasma-derived extracellular vesicles (pEVs) are emerging as promising nanotherapeutics owing to their immunomodulatory and regenerative potential. However, co-isolated lipoproteins may influence their biological activity. This study investigated how purification to reduce lipoprotein-associated material affects the immunomodulatory and pro-regenerative properties of pEVs.

Methods: pEVs were isolated by tangential flow filtration following styrene-maleic acid (SMA) pre-treatment to disrupt lipoproteins. Their physicochemical characteristics and immunomodulatory effects on RAW264.7 macrophages were compared with those of unpurified pEVs. The effects of conditioned medium from macrophages treated with either unpurified pEVs or purified pEVs on the differentiation and mineralisation of human periodontal ligament cells (hPDLCs) were also evaluated.

[1]School of Dentistry, Centre for Orofacial Regeneration, Reconstruction and Rehabilitation (COR3), The University of Queensland, Brisbane 4072, Australia.
[2]School of Chemical Engineering, The University of Queensland, Brisbane 4072, Australia.
[3]Australian Institute for Bioengineering and Nanotechnology, The University of Queensland, Brisbane 4072, Australia.
[4]Herston Biofabrication Institute, The University of Queensland and Metro North Health, Brisbane 4029, Australia.

Correspondence to: Prof. Sašo Ivanovski, Dr. Yinghong Zhou, School of Dentistry, Centre for Orofacial Regeneration, Reconstruction and Rehabilitation (COR3), The University of Queensland, Brisbane 4072, Australia. E-mail: s.ivanovski@uq.edu.au; yinghong.zhou@uq.edu.au; Prof. Joy Wolfram, School of Chemical Engineering, The University of Queensland, Brisbane 4072, Australia. E-mail: j.wolfram@uq.edu.au

Results: Purification reduced apolipoprotein abundance while retaining EV-associated markers and vesicular morphology. Both preparations attenuated inflammatory responses in lipopolysaccharide-stimulated RAW264.7 macrophages. Purified pEVs induced greater changes in selected macrophage phenotype markers and reduced nuclear p65 localisation, whereas unpurified pEVs suppressed some cytokine readouts more strongly. Conditioned medium from purified pEV-treated macrophages significantly enhanced hPDLC mineralisation and increased the expression of selected bone- and cementum-associated genes.

Conclusion: These findings link SMA-based purification to distinct immunomodulatory effects and enhanced differentiation-associated responses *in vitro*, supporting further investigation of purified pEVs for periodontal tissue regeneration.

INTRODUCTION

Periodontitis is an inflammatory disease induced by a polymicrobial biofilm infection, which disrupts host immune regulation and leads to the destruction of periodontal tissues that anchor teeth. Periodontitis is a leading contributor to tooth loss among adults and has been linked to an elevated risk of systemic conditions, including cardiovascular disease, Alzheimer's disease and diabetes[1,2]. A hallmark of disease progression is the predominance of pro-inflammatory macrophages within the periodontal environment[3]. Effective treatment requires sustained resolution of inflammation to enable the restoration of the physiological structure and function of the periodontium. Nevertheless, conventional approaches to periodontal treatment, including scaling and root surface debridement, offer only temporary microbial reduction and are inadequate for predictably achieving long-term inflammation resolution or tissue regeneration[4,5].

These challenges have encouraged the development of novel therapeutic approaches aimed at promoting tissue regeneration under inflammatory conditions. Among these, extracellular vesicles (EVs) have attracted increasing attention for their potential applications in disease diagnosis and treatment[6-8], as changes in EV abundance and molecular composition are highly associated with disease progression[9]. EVs are particles released by cells that range in size from the nanometre to the micrometre scale and are enclosed by a lipid bilayer and contain various bioactive components, such as lipids, proteins, and nucleic acids[10,11]. Upon release into the extracellular environment, they transport these biomolecules to regulate the activity of recipient cells, playing a role as key mediators of communication between cells[12]. In addition to facilitating intercellular communication, EVs derived from stem cells also demonstrate the ability to modulate macrophage activity and promote tissue regeneration, supporting their use as a cell-free alternative to stem cell transplantation[13-16].

Practical challenges in stem cell sourcing and EV production have prompted interest in more accessible sources, including human plasma[17]. Plasma is widely recognised as a practical and cost-effective source for both diagnostic and therapeutic applications[18,19]. As a biological fluid that circulates systemically, plasma serves as a reservoir for delivering disease-modulating factors[17]. Recent research highlights that plasma-derived EVs (pEVs) have emerged as promising non-invasive biomarkers for the early diagnosis of neurodegenerative and inflammatory diseases[20]. Beyond their diagnostic potential, pEVs are increasingly being explored as advanced therapeutic tools for tissue regeneration. In particular, platelet-rich pEVs have demonstrated significant potential in bone and cartilage repair through the delivery of concentrated growth factors[21,22]. Notably, pEVs are capable of homing to inflamed tissues, where they can suppress the release of pro-inflammatory cytokines while promoting tissue regeneration in preclinical disease models, such as intervertebral disc degeneration[23]. In addition, these vesicles, originating from plasma exudates associated with increased endothelial permeability, have been shown to promote anti-inflammatory responses and enhance efferocytosis[24]. These findings motivate investigation of pEV preparations in periodontal repair, where inflammation and tissue differentiation are closely linked.

A major technical challenge, however, is the co-isolation of other biological nanoparticles such as lipoproteins, which overlap with EVs in size and can influence their measured biological activity. Reducing these co-isolated components improves the interpretation and reproducibility of functional analyses, thereby maximising their therapeutic potential[25]. Although pEVs have been reported to regulate macrophage inflammatory responses, how lipoprotein depletion influences downstream periodontal ligament cell responses remains unclear[24]. In the present study, we applied styrene-maleic acid (SMA) pre-treatment followed by tangential flow filtration (TFF) and diafiltration, adapting a reported lipoprotein depletion method compatible with scalable processing[25]. We compared preparations isolated with and without SMA pre-treatment for their effects on macrophage inflammatory responses and subsequent differentiation of human periodontal ligament cells. This approach examines purification-associated functional differences and provides a basis for further mechanistic studies and *in vivo* evaluation of periodontal repair.

METHODS

Isolation of pEVs and purified pEVs by tangential flow filtration

pEVs were isolated from de-identified residual plasma from healthy donors provided by the Australian Red Cross Lifeblood, with approval from the University of Queensland Human Research Ethics Committee (Approval No. 2022/HE000652). Plasma was collected using citrate phosphate dextrose-adenine (CPDA-1) as the anticoagulant. The plasma samples were preserved at -80 °C for up to 1 year. Prior to EV isolation, 1-5 mL plasma samples were centrifuged at 800 × *g* for 30 min using an Eppendorf 5810 R centrifuge (Eppendorf, Hamburg, Germany) to remove large particulates. Following centrifugation, the lipid-rich upper layer was carefully discarded. For the unpurified pEV preparation, 400 µL of clarified plasma was mixed with 720 mL of phosphate-buffered saline (PBS), corresponding to a plasma-to-PBS ratio of 1:1,800 (v/v) and a total volume of 720.4 mL.

Plasma pre-treatment to generate purified pEVs was adapted from previously reported protocols with minor adjustments[25]. Briefly, Lipodisq® styrene-maleic acid copolymer (SMA) 2:1 (Merck, Darmstadt, Germany) was added to 1 mL of clarified plasma at 20 mg/mL (2% w/v), corresponding to a nominal polymer concentration of 2 mM based on the manufacturer-reported weight-average molecular weight of approximately 10 kDa. The mixture was gently stirred at 4 °C for 12 h to allow equilibration. Subsequently, 400 µL of SMA-treated plasma was mixed with 720 mL of PBS, giving the same plasma-to-PBS ratio and total volume as the untreated pEV preparation.

Both diluted preparations were processed using the KrosFlo® Research 2i Tangential Flow Filtration System (Repligen, Waltham, Massachusetts, US), with modifications to previously established protocols[25]. Briefly, diluted plasma was sequentially filtered through sterile modified polyethersulfone hollow fibre membranes with a pore size cut-off of 0.65 µm and a molecular weight cut-off of 750 kDa to remove large and small components, such as debris and non-EV-associated proteins, respectively[26,27]. All membranes were pre-conditioned with PBS and cleaned after use with 5 mM NaOH, followed by rinsing with PBS. The feed flow rate was maintained between 50 and 60 mL/min to keep the feed flow shear rate at or below 2,000 s^{-1} to minimise shear stress.

During filtration, the diluted plasma was concentrated from 720.4 mL to 50 mL. The retained EV fraction underwent six rounds of diafiltration using a 750 kDa membrane against a cryoprotective buffer containing 5% (w/v) sucrose, 50 mM Tris, and 2 mM $MgCl_2$[28], and was then concentrated from 50 mL to approximately 10 mL, aliquoted, and stored at -80 °C until further analysis. EVs isolated from SMA-treated plasma were designated as purified pEVs, whereas those isolated from untreated plasma were designated as pEVs. Identical plasma volumes and dilution procedures were used for both preparations.

Nanoparticle tracking analysis

Particle size distribution and concentration were characterised by nanoparticle tracking analysis (NTA) using a NanoSight Pro (Malvern Panalytical). The instrument was equipped with NanoSight NS XPLORER software (version 1.1.0.6) and a 642 nm laser. For each sample, three videos were recorded and analysed using automated camera settings and capture durations. Camera settings and detection thresholds were configured automatically by the instrument.

Cryogenic transmission electron microscopy

Cryogenic transmission electron microscopy (cryo-TEM) was conducted to visualise lipid bilayers characteristic of EVs. An EV suspension (3 μL) was applied to carbon-coated perforated Lacey formvar films on 200-mesh copper grids (Electron Microscopy Services) and excess liquid was removed. Samples were vitrified by plunging into liquid ethane (-182.8 °C) with a Leica EM GP2 automated plunge freezer (Leica, Germany), with the chamber maintained at 22 °C and 95% relative humidity. The specimens were then maintained in liquid nitrogen prior to examination. Cryo-TEM imaging was conducted on a JEOL Cryo ARM 300 (JEM-Z300FSC) TEM microscope operating at 300 kV and incorporating a cold field emission gun (FEG) and an in-column Omega energy filter. Images were acquired in zero-loss mode with a 20 eV energy-selecting slit under low-electron-dose conditions using a Gatan K3 direct electron detector and SerialEM software[29].

Enzyme-linked immunosorbent assay

Enzyme-linked immunosorbent assays (ELISAs) were performed using kits from R&D Systems (Minneapolis, MN, USA), according to the manufacturer's instructions, to quantify human apolipoprotein A-I (ApoA-I), human apolipoprotein B-100 (ApoB-100), mouse tumour necrosis factor-α (TNF-α), and mouse interleukin-1β (IL-1β).

Micro-bicinchoninic acid assay

The total protein content of pEV samples was determined using the Pierce™ Micro BCA Protein Assay (Thermo Fisher Scientific, Australia) in accordance with the manufacturer's protocol.

Western blotting

Western blotting was performed to characterise EV-associated proteins according to a previously established protocol[27]. Total protein concentrations were determined using a BCA assay, and samples were normalised to ensure equal protein loading. For each sample, 10.21 μg of protein was heated at 90 °C for 5 min and separated on a 4%-12% Bis-Tris gel using NuPage™ MOPS SDS running buffer (Thermo Fisher Scientific, Massachusetts, USA) at 120 V for 1.5-2 h. The proteins were electrotransferred to nitrocellulose membranes at 200 mA for 1.5 h in NuPAGE™ transfer buffer (Thermo Fisher Scientific, Massachusetts, USA). Membranes were blocked at room temperature with 5% (w/v) milk in Tris-buffered saline containing 0.1% Tween (TBST; Thermo Fisher Scientific, Massachusetts, USA), followed by overnight incubation at 4 °C with primary antibodies targeting CD63 (Abcam, Cambridge, United Kingdom), Alix (Cell Signaling Technology, Massachusetts, USA), and apolipoprotein E (ApoE; Invitrogen, Massachusetts, USA), diluted 1:250-1:500 in TBST containing 1% (w/v) milk. After washing with TBST, the membranes were incubated with the corresponding secondary antibodies (1:3,000) for 2 h at room temperature. Protein bands were visualised using the SuperSignal West Femto kit and captured by the ChemiDoc MP Imaging System (Bio-Rad, Hercules, California, USA).

For signalling pathway analysis, protein samples (25 μg per lane) were heated at 90 °C for 5 min before electrophoretic separation on 4%-20% polyacrylamide gels using Tris/glycine/SDS running buffer at 120 V for 1.5 h (Bio-Rad, Hercules, California, USA). Proteins were subsequently electrotransferred to

polyvinylidene difluoride (PVDF) membranes at 300 mA for 1 h. After blocking with Odyssey blocking buffer (#927-40000, LI-COR Biosciences) at room temperature, membranes were incubated with primary antibodies against total nuclear factor-κB (NF-κB) p65 (#8242, Cell Signaling Technology), β-Actin (#4970, Cell Signaling Technology), and phosphorylated p65 (Ser536; #3033, Cell Signaling Technology), each diluted 1:1,000 in Odyssey blocking buffer at 4 °C overnight. After washing with TBS, membranes were incubated with IRDye 800CW-conjugated donkey anti-rabbit IgG (#925-32213, LI-COR Biosciences; 1:5,000) for 1 h at room temperature. Images were visualised and recorded using a ChemiDoc MP Imaging System (Bio-Rad).

Cells and reagents

The murine macrophage cell line RAW264.7 (RAW) was sourced from The American Type Culture Collection (ATCC; TIB-71; RRID: CVCL_0493). Cell identity was verified using the authentication records provided by ATCC. Cells were cultured in Dulbecco's modified Eagle's medium (DMEM; Gibco, Thermo Fisher Scientific, Australia) supplemented with 10% fetal bovine serum (FBS) and 1% antibiotic-antimycotic (A/A) at 37 °C in a humidified incubator containing 5% CO_2. Cells at passages 5-15 were used for experiments.

Human periodontal ligament cells (hPDLCs) were obtained from periodontally healthy wisdom teeth, with ethical approval from the University of Queensland Human Research Ethics Committee (Approval No. 2019/HE000134). Their phenotype was characterised by flow cytometry, with positive expression of the mesenchymal stromal cell-associated markers CD105, CD73 and CD90, and negative expression of CD19, CD34 and CD45. Differentiation potential was confirmed by lineage-specific staining. Cells were cultured in DMEM supplemented with 10% FBS and 1% A/A. For osteogenic differentiation, hPDLCs were cultured in human osteoblast differentiation medium (#417D-250, Sigma). Only early-passage cells (P2-P3) were used for experiments.

RAW cells and hPDLCs were screened for mycoplasma contamination using the MycoAlert® Mycoplasma Detection Kit (#LT07-318, Lonza, Australia) according to the manufacturer's instructions. Both cell types tested negative.

Cell viability and material-stimulated cell performance

Cell viability was assessed using the Alamar Blue HS Cell Viability reagent (#A50100, Invitrogen, Thermo Fisher Scientific, USA) and Live/Dead assay (Sigma-Aldrich, Australia). RAW cells and hPDLCs were seeded separately in 96-well plates at 5×10^3 cells per well and allowed to attach overnight. Then, cells were cultured with different concentrations of pEVs or purified pEVs in complete culture medium, and viability was assessed after 1 and 3 days. Images were acquired by a confocal laser scanning microscope (Nikon C2 + Ti-E).

To evaluate the immunomodulatory effects, RAW cells (2×10^5) were seeded in 24-well plates and allowed to attach overnight. Cells were stimulated with 1 μg/mL lipopolysaccharide (LPS; *In Vitro* Technologies, Australia) for 2 h to induce a pro-inflammatory M1 phenotype. After washing three times with PBS to remove residual LPS, cells were stimulated with 100 ng/mL LPS, either alone or in combination with pEVs or purified pEVs for a further 24 h. For lipoprotein reconstitution experiments, purified pEVs were supplemented with low-density lipoprotein (LDL, #SAE0053, Merck Life Science, Australia) and high-density lipoprotein (HDL, #L8039, Merck Life Science, Australia), mixed at an LDL:HDL ratio of 35:65 by protein mass, at a final combined lipoprotein concentration of 100 μg/mL.

Table 1. Primer sequences used for RT-qPCR

Mouse gene	Forward (5′ to 3′)	Reverse (5′ to 3′)
Gapdh	GTGTCCGTCGTGGATCTGA	CCTGCTTCACCACCTTCTTG
Il1b	TGGAGAGTGTGGATCCCAAG	GGTGCTGATGTACCAGTTGG
Il6	ATAGTCCTTCCTACCCCAATTTCC	GATGAATTGGATGGTCTTGGTCC
Tnf	CTGAACTTCGGGGTGATCGG	GGCTTGTCACTCGAATTTTGAGA
Osm	ACGGTCCACTACAACACCAG	CCATCGTCCCATTCCCTGAAG
Ccr7	GGTGGTGGCTCTCCTTGTCA	CGTGGTATTCTCGCCGATGT
Cd86	CTGCTCATCATTGTATGTCAC	ACTGCCTTCACTCTGCATTTG
Nos2	CACCAAGCTGAACTTGAGCG	CGTGGCTTTGGGCTCCTC
Human gene	**Forward (5′ to 3′)**	**Reverse (5′ to 3′)**
GAPDH	GGAGCGAGATCCCTCCAAAAT	GGCTGTTGTCATACTTCTCATGG
ALP	TAAGGACATCGCCTACCAGCTC	TCTTCCAGGTGTCAACGAGGT
OCN	GCAAAGGTGCAGCCTTTGTG	GGCTCCCAGCCATTGATACAG
OPN	TCACCTGTGCCATACCAGTTAA	TGAGATGGGTCAGGGTTTAGC
CEMP1	GGGCACATCAAGCACTGACAG	CCCTTAGGAAGTGGCTGTCCAG
CAP	CTGCGCGCTGCACATGG	GCGATGTCGTAGAAGGTGAGCC
BSP	AGGCTGAGAATACCACACTTTC	GGATTGCAGCTAACCCTGTAT

ALP: Alkaline phosphatase; *BSP*: bone sialoprotein; *CAP*: cementum attachment protein; *Ccr7*: C-C Motif Chemokine Receptor 7; *Cd86*: cluster of differentiation 86; *CEMP1*: cementum protein 1; *Il1b*: interleukin-1; *Il6*: interleukin-6; *Gapdh/GAPDH*: glyceraldehyde-3-phosphate dehydrogenase; *Nos2*: nitric oxide synthase 2; *OCN*: osteocalcin; *OPN*: osteopontin; *Osm*: oncostatin M; RT-qPCR: reverse transcription quantitative polymerase chain reaction; *Tnf*: tumour necrosis factor-α.

To investigate pro-regenerative effects, conditioned medium (CM) was collected from LPS-primed RAW cells following treatment. After 24 h of stimulation, cells were washed three times with PBS and incubated in serum-free DMEM at 37 °C for an additional 6 h. The collected CM was centrifuged at 300 × g for 10 min to remove residual cells and debris, then filtered through a 0.22 μm membrane. No additional EV-specific depletion procedure was performed before the CM was applied to hPDLCs. For osteogenic differentiation experiments, hPDLCs (2×10^5) were plated in 24-well plates and maintained in a 1:1 mixture of CM from pEV-treated or purified pEV-treated macrophages and osteogenic medium, with medium replaced every 3 days. hPDLCs cultured in osteogenic medium alone served as the positive control (CN+).

Reverse transcription quantitative polymerase chain reaction (RT-qPCR)

Total RNA was isolated using TRIzol™ reagent (Life Technologies Australia) from RAW cells and hPDLCs treated with RAW cell-derived CM. Total RNA (500 ng) was reverse-transcribed into complementary DNA (cDNA) using the First Strand cDNA Synthesis Kit (#K1612, Thermo Fisher Scientific, Australia). Subsequent quantitative PCR (qPCR) analysis was conducted using a StepOnePlus Real-Time PCR System (Life Technologies Australia) to assess the expression of inflammatory and osteogenic markers. Primers were designed using cDNA sequences from the NCBI database [Table 1]. Three independent experiments were performed, with each reaction run in technical triplicate. For each independent experiment, the mean of three technical replicates was calculated and used for subsequent statistical analysis. Gene expression was normalised against the housekeeping gene *Gapdh* in RAW cells and *GAPDH* in hPDLCs.

Immunofluorescence staining

RAW cells (3×10^4) were seeded in 24-well plates and allowed to attach overnight. Following exposure to pEVs or purified pEVs, cells were fixed with 4% paraformaldehyde (PFA) for 15 min, followed by membrane permeabilisation using 0.25% Triton X-100 for 10 min. Non-specific antibody binding was minimised by

blocking with 4% bovine serum albumin (BSA) for 1 h at room temperature. Subsequently, cells were incubated with primary antibodies targeting inducible nitric oxide synthase (iNOS) (#ab3523, Abcam, 1:50), arginase 1 (Arg1) (#93668, Cell Signalling Technology, 1:50), CD206 (#ab64693, Abcam, 1:1,000) and NF-κB p65 (#D14E12, Cell Signalling Technology, 1:1,000) overnight at 4 °C. After washing, cells were exposed for 1 h to the Alexa Fluor 488- or Alexa Fluor 568-labelled goat anti-rabbit IgG secondary antibodies (Sigma-Aldrich, Australia), followed by nuclear staining with 4',6-diamidino-2-phenylindole (DAPI) for 1 h. Images were obtained by the confocal laser scanning microscope (Nikon C2 + Ti-E).

Alizarin Red S staining

Mineralised matrix formation was assessed using Alizarin Red S staining on days 14 and 21 of osteogenic differentiation in hPDLCs cultured with CM from RAW cells treated with pEVs or purified pEVs. Cells were fixed with 4% PFA for 15 min before 20 min of incubation with Alizarin Red S (ARS) solution (#2003999, Sigma-Aldrich, Australia). Excess stain was washed thoroughly with sterile water. For semi-quantitative analysis, bound dye was extracted by incubating the stained cell monolayers with 50% (w/v) acetic acid for 10 min with gentle shaking, followed by neutralisation with 4 M NaOH. For spectrophotometric quantification, 200 µL of each extracted dye solution was dispensed into a 96-well plate, and the absorbance was recorded at 405 nm.

Biological replicates and statistical analysis

pEVs and purified pEVs were isolated from plasma obtained from three independent donors (n = 3), without pooling samples across donors. For cell-based assays involving RAW cells and hPDLCs, three independent experiments were performed, with each experiment using pEVs and purified pEVs derived from a different plasma donor. All hPDLC experiments used cells derived from the same donor. RT-qPCR, ELISA, and Western blot assays were performed in technical triplicate within each independent experiment. The three technical measurements were averaged to generate one representative value per condition for each independent experiment, which was subsequently used for statistical analysis. Statistical analyses were performed using these three independent values (n = 3), representing three plasma donor-level biological replicates.

GraphPad Prism version 9.0 (GraphPad Software, San Diego, CA, USA) was used to perform statistical analyses. Statistical differences among three or more groups were determined using one-way ANOVA followed by Tukey's post hoc test for multiple comparisons, while Student's t-test was applied to two-group comparisons. Results were considered statistically significant when the P value was < 0.05.

RESULTS

Characterisation of pEVs and purified pEVs

pEV preparations were isolated by TFF with or without SMA pre-treatment, adapting a previously reported method to reduce co-isolated lipoproteins[25]. EV characterisation included particle analysis, protein markers and vesicle morphology, informed by the International Society of Extracellular Vesicles recommendations[30,31]. Specifically, particle concentration and size distribution of pEVs and purified pEVs were evaluated using NTA. The analysis revealed particle concentrations of $(1.51 \pm 0.29) \times 10^{10}$ particles/mL for pEVs and $(2.08 \pm 0.27) \times 10^{10}$ particles/mL for purified pEVs [Figure 1A]. Both groups exhibited similar size modes, with an average mode size of approximately 150 nm, and fell within the expected EV size range of 50-300 nm [Figure 1A and B].

Western blotting detected the EV-associated proteins Alix and CD63 in both preparations, with stronger bands in purified pEVs under equal protein loading [Figure 1C]. Apolipoprotein E (ApoE) abundance was lower after purification [Figure 1C], as were the ApoB-100 and ApoA-I signals measured by ELISA

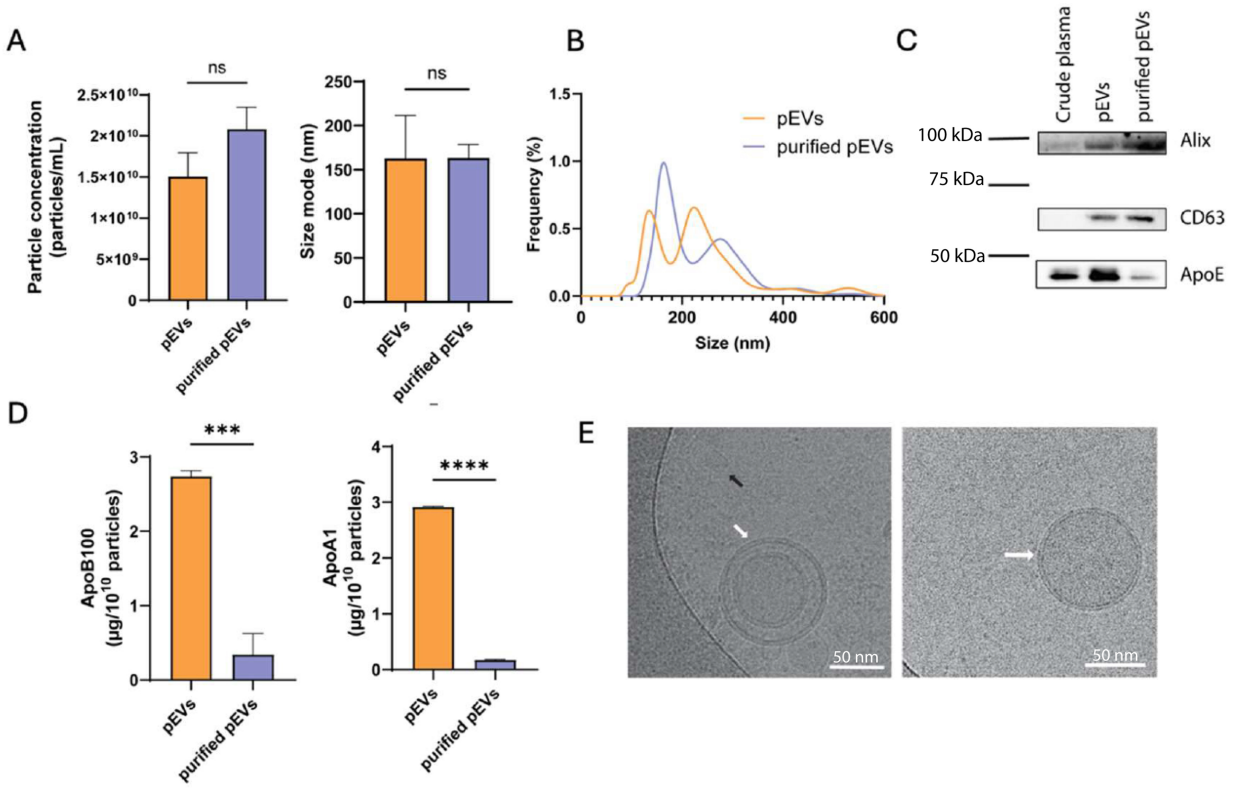


Figure 1. EVs were characterised using NTA to determine (A) particle concentration and size mode, and (B) size distribution. (C) Western blot of EV markers (Alix and CD63) and ApoE as a lipoprotein-associated protein alongside (D) levels of ApoB-100 and ApoA-I evaluated by ELISA. (E) Cryo-TEM images of individual EVs (white arrow) and lipoprotein components (black arrow). Data are presented as mean ± SD. Data in (A) represent technical replicates from a single plasma donor, whereas all other experimental data (B-E) were obtained from three independent biological replicates (n = 3). The corresponding original, uncropped Western blot images are presented in Supplementary Figure 3. Statistical significance is indicated as ns; ***P < 0.001; ****P < 0.0001. Alix: ALG-2-interacting protein X; ApoA-I: apolipoprotein A-I; ApoB-100: apolipoprotein B-100; ApoE: apolipoprotein E; CD63: cluster of differentiation 63; cryo-TEM: cryogenic transmission electron microscopy; ELISA: enzyme-linked immunosorbent assay; EVs: extracellular vesicles; ns: non-significant; NTA: nanoparticle tracking analysis; pEVs: plasma-derived extracellular vesicles; SD: standard deviation.

[Figure 1D]. The reduction in ApoA-I is consistent with depletion of HDL-associated material alongside ApoB-containing lipoproteins. Cryo-TEM revealed lipid bilayer structures characteristic of EVs in both preparations (white arrows; Figure 1E)[11]. In the unpurified preparation, a smaller particle, approximately 18-23 nm in diameter, exhibited morphology consistent with LDL (black arrow; Figure 1E)[32,33]. No comparable lipoprotein-like structures were evident in the representative purified pEV images, consistent with the apolipoprotein measurements and previous findings[25].

Cell biocompatibility and anti-inflammatory properties of pEVs and purified pEVs

The cytocompatibility of pEVs and purified pEVs was assessed using the Alamar Blue assay after one and three days of exposure. Three concentrations were tested: 1×10^7, 1×10^8 and 1×10^9 particles/mL [Supplementary Figure 1A and B]. The highest tested concentration maintained viability in both RAW cells and hPDLCs and was selected for subsequent functional assays. At this concentration, Alamar Blue signals increased in RAW cells at selected time points [Figure 2A] and remained comparable to controls in hPDLCs [Figure 2B]. Live/Dead staining likewise showed no detectable reduction in viability in either cell type [Figure 2C and D]. These results support the cytocompatibility of both preparations at 1×10^9 particles/mL over the observation period.

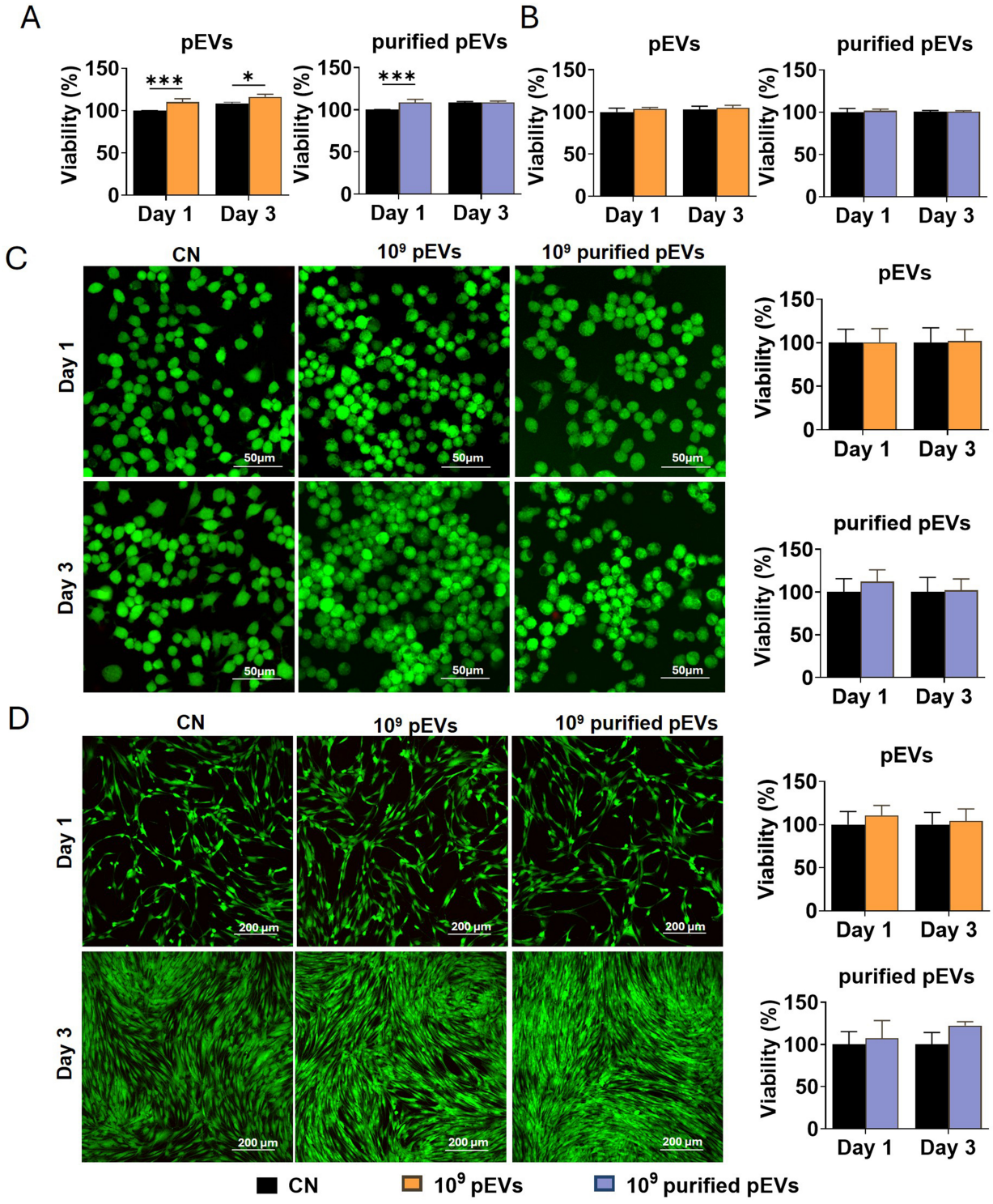


Figure 2. Effects of pEVs and purified pEVs on the viability of RAW cells and hPDLCs. Alamar Blue assays showing the viability of (A) RAW cells and (B) hPDLCs on days 1 and 3 following treatment with pEVs or purified pEVs at 1 × 10^9 particles/mL. Representative Live/Dead staining images of (C) RAW cells and (D) hPDLCs on days 1 and 3, with FDA labelling live cells in green and PI labelling dead cells in red, accompanied by quantitative analysis of fluorescence intensity. Data are expressed as the mean ± SD of three independent experiments, each using paired pEV and purified pEV preparations from a different plasma donor (n = 3). Statistical significance is indicated as $^{*}P < 0.05$; $^{**}P < 0.01$; $^{***}P < 0.001$. EVs: Extracellular vesicles; FDA: fluorescein diacetate; hPDLCs: human periodontal ligament cells; pEVs: plasma-derived extracellular vesicles; PI: propidium iodide; RAW: RAW264.7 macrophages; SD: standard deviation.

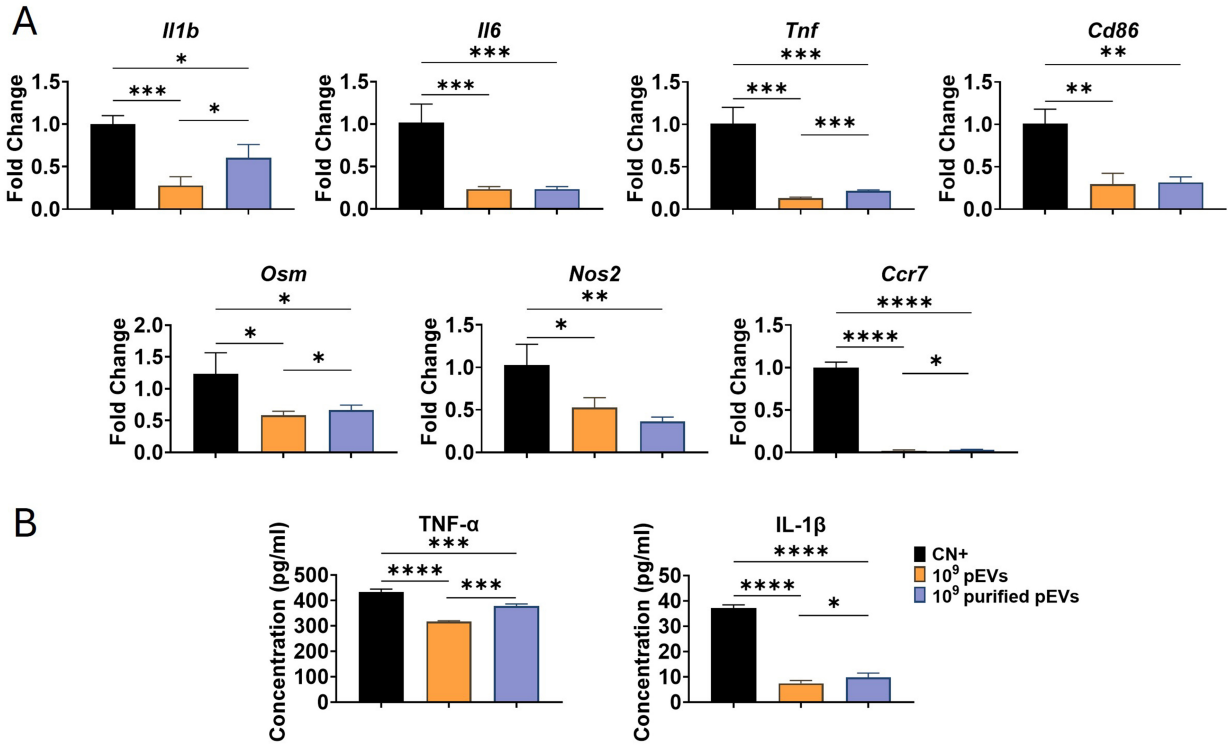


Figure 3. Immunoregulatory effects of pEVs and purified pEVs on RAW cells. (A) Fold changes in pro-inflammatory marker expression in RAW cells pre-stimulated with *E. coli* LPS (1 μg/mL) for 2 h, washed three times with PBS, and subsequently stimulated with 100 ng/mL LPS, either alone or in combination with pEVs or purified pEVs (1×10^9 particles/mL) for 24 h; (B) Concentrations of TNF-α and IL-1β in the culture medium of LPS-stimulated RAW cells. Data are expressed as the mean ± SD of three independent experiments, each using paired pEV and purified pEV preparations from a different plasma donor ($n = 3$). Statistical significance is indicated as $^{*}P < 0.05$; $^{**}P < 0.01$; $^{***}P < 0.001$; $^{****}P < 0.0001$. IL-1β: Interleukin-1β; *Il6*: interleukin-6; *Ccr7*: C-C Motif Chemokine Receptor 7; *Cd86*: Cluster of differentiation 86; LPS: lipopolysaccharide; *Nos2*: nitric oxide synthase 2; *Osm*: Oncostatin M; pEVs: plasma-derived extracellular vesicles; PBS: phosphate-buffered saline; RAW: RAW264.7 macrophages; SD: standard deviation; TNF-α: tumour necrosis factor-α.

Both pEV preparations reduced inflammatory gene expression in LPS-stimulated RAW cells relative to the LPS-only control [Figure 3A]. ELISA also showed lower TNF-α and IL-1β concentrations, with greater suppression by unpurified pEVs [Figure 3B]. Lipoprotein reconstitution of purified pEVs significantly reduced *Osm* expression and shifted other measured transcripts numerically towards levels observed with unpurified pEVs [Supplementary Figure 2]. These results suggest that co-isolated lipoproteins contribute to selected anti-inflammatory effects, although independent effects of SMA treatment cannot be excluded. Overall, both preparations attenuated inflammatory responses, with compositional differences potentially contributing to their distinct immunomodulatory profiles.

Macrophage phenotype-associated markers were assessed by immunofluorescence staining [Figure 4]. Semi-quantitative analysis showed that both pEV preparations significantly reduced iNOS fluorescence and increased Arg1 and CD206 fluorescence relative to the LPS-only control. Purified pEVs produced greater changes in iNOS and Arg1 than unpurified pEVs, supporting a more pronounced shift towards an M2-like marker profile.

To further investigate the anti-inflammatory effects of purified pEVs, NF-κB signalling was assessed by immunofluorescence staining and Western blotting. Immunofluorescence analysis showed that purified pEV treatment markedly reduced nuclear p65 localisation [Figure 5A]. Western blotting analysis further supported the attenuation of NF-κB activation, as evidenced by decreased levels of phosphorylated p65 (p-p65) [Figure 5B]. Collectively, these findings are consistent with attenuated NF-κB-associated signalling and suggest its possible involvement in the anti-inflammatory response to purified pEVs.

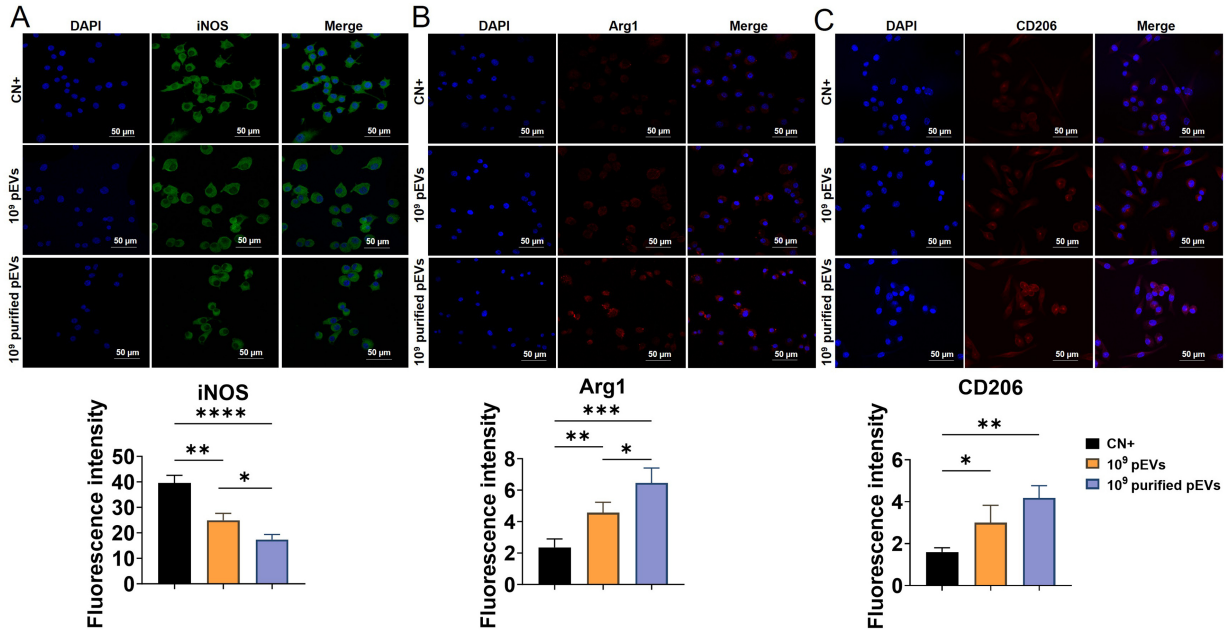


Figure 4. Effects of pEVs and purified pEVs on macrophage phenotype-associated markers. RAW cells were primed with *E. coli* LPS (1 μg/mL) for 2 h, washed three times with PBS, and subsequently stimulated with 100 ng/mL LPS, either alone or in combination with pEVs or purified pEVs (1 × 10^9 particles/mL) for 24 h. Representative immunofluorescence images and corresponding quantification of fluorescence intensity for (A) iNOS (green), (B) Arg1 (red), and (C) CD206 (red). Nuclei were stained with DAPI (blue). Data are expressed as the mean ± SD of three independent experiments, each using paired pEV and purified pEV preparations from a different plasma donor (n = 3). Statistical significance is indicated as $^{*}P < 0.05$; $^{**}P < 0.01$; $^{***}P < 0.001$; $^{****}P < 0.0001$. Arg1: Arginase 1; CD206: cluster of differentiation 206; DAPI: 4′,6-diamidino-2-phenylindole; iNOS: inducible nitric oxide synthase; LPS: lipopolysaccharide; pEVs: plasma-derived extracellular vesicles; PBS: phosphate-buffered saline; RAW: RAW264.7 macrophages; SD: standard deviation.

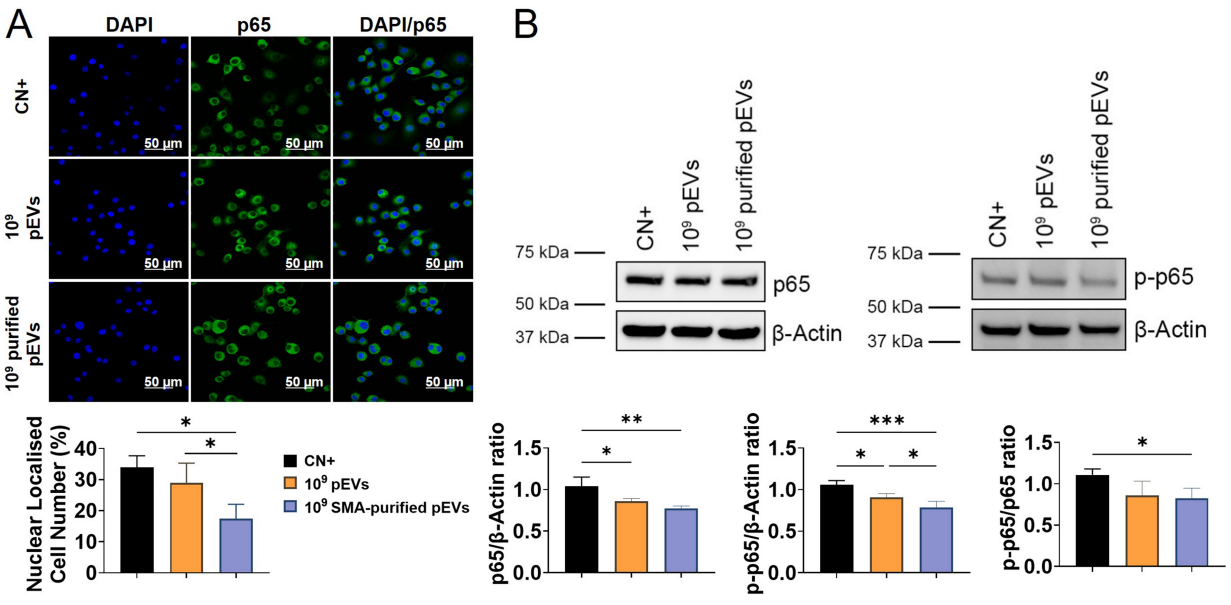


Figure 5. Effects of pEVs and purified pEVs on NF-κB-associated signalling in RAW cells. RAW cells were primed with *E. coli LPS* (1 μg/mL) for 2 h, washed three times with PBS, and subsequently stimulated with 100 ng/mL LPS, either alone or in combination with pEVs or purified pEVs (1 × 10^9 particles/mL) for 24 h. (A) Representative immunofluorescence images showing p65 nuclear localisation and quantitation of the proportion of RAW cells with nuclear p65 localisation; (B) Representative Western blots of total p65, p-p65 and β-Actin, with corresponding densitometric analysis. The corresponding original, uncropped Western blot images are presented in Supplementary Figure 4. Data are expressed as the mean ± SD of three independent experiments, each using paired pEV and purified pEV preparations from a different plasma donor (n = 3). Statistical significance is indicated as $^{*}P < 0.05$; $^{**}P < 0.01$; $^{***}P < 0.001$. DAPI: 4′,6-diamidino-2-phenylindole; LPS: lipopolysaccharide; NF-κB: nuclear factor-κB; p65: nuclear factor-κB p65; p-p65: phosphorylated p65; pEVs: plasma-derived extracellular vesicles; PBS: phosphate-buffered saline; SD: standard deviation.

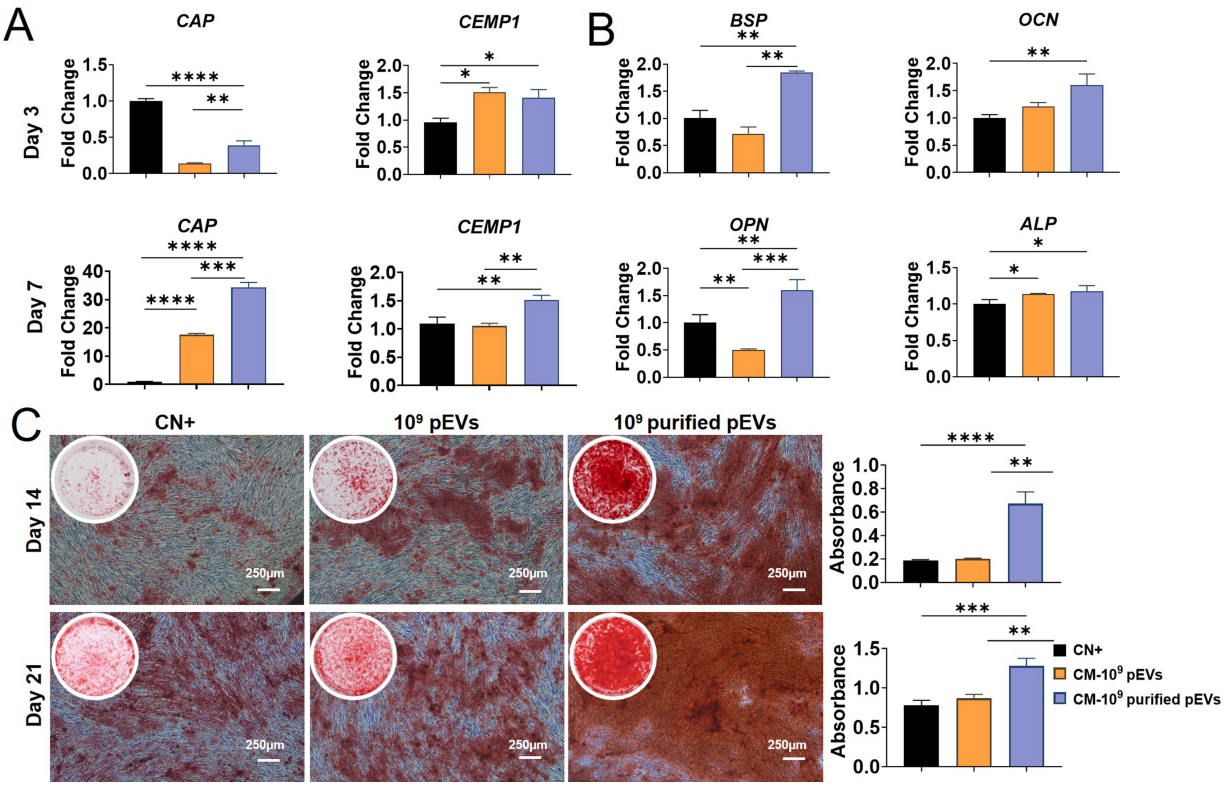


Figure 6. Cementogenic and osteogenic differentiation-associated responses of hPDLCs to macrophage-derived conditioned medium. hPDLCs were cultured in a 1:1 mixture of osteogenic medium and CM from LPS-stimulated macrophages treated with pEVs or purified pEVs at 1 × 10^9 particles/mL. (A) Expression of cementum-associated markers CAP and CEMP1 on days 3 and 7; (B) Expression of osteogenesis-related markers, including BSP, OCN, OPN and ALP on day 3; (C) Representative ARS staining images and quantification of mineralisation on days 14 and 21. Quantification was performed by measuring the absorbance of the extracted dye. Data are expressed as the mean ± SD of three independent experiments, each using paired pEV and purified pEV preparations from a different plasma donor (n = 3). Statistical significance is indicated as $^{*}P < 0.05$; $^{**}P < 0.01$; $^{***}P < 0.001$; $^{****}P < 0.0001$. *ALP*: Alkaline phosphatase; ARS: Alizarin Red S; *BSP*: bone sialoprotein; *CAP*: cementum attachment protein; *CEMP1*: cementum protein 1; CM: conditioned medium; hPDLCs: human periodontal ligament cells; LPS: lipopolysaccharide; *OCN*: osteocalcin; *OPN*: osteopontin; pEVs: plasma-derived extracellular vesicles; SD: standard deviation.

Conditioned medium from purified pEV-treated macrophages enhances hPDLC mineralisation

hPDLCs were cultured with CM from LPS-stimulated macrophages treated with pEVs or purified pEVs. Both CM treatments promoted the upregulation of key regulators of tooth root cementum repair, with cementum protein 1 (*CEMP1*) expression elevated on day 3. However, only the purified pEV group showed increased expression relative to control on day 7 [Figure 6A]. Cementum attachment protein (*CAP*) transcript levels decreased on day 3 in both treatment groups, but subsequently exceeded levels in the control group on day 7, with a significantly greater increase in the purified pEV group [Figure 6A].

On day 3, hPDLCs exposed to CM from purified pEV-treated macrophages showed significantly higher expression of typical osteogenic markers including bone sialoprotein (*BSP*), osteocalcin (*OCN*), osteopontin (*OPN*), and alkaline phosphatase (*ALP*) than the osteogenic medium control [Figure 6B]. In contrast, CM from unpurified pEV-treated macrophages reduced the expression of both *BSP* and *OPN*, suggesting the functional impact of lipoprotein components on downstream cellular responses. These transcriptional findings were supported by ARS staining, which showed significantly greater mineralised nodule formation in the purified pEV-CM group than in the control and unpurified pEV-CM groups on days 14 and 21

[Figure 6C]. Quantification of ARS staining further confirmed the superior mineralisation response induced by CM from purified pEV-treated macrophages [Figure 6C]. These results demonstrate that CM from purified pEV-treated macrophages enhances hPDLC mineralisation and modulates bone- and cementum-associated gene expression *in vitro*.

DISCUSSION

Purification and functional interpretation of pEV preparations

pEVs have attracted substantial interest as a potential cell-free approach to tissue regeneration owing to their natural abundance, accessibility and immunomodulatory properties[17,34]. However, plasma is a highly complex fluid containing diverse proteins, cytokines, lipoproteins, nucleic acids, and heterogeneous EV populations, making preparation composition an important consideration in functional studies[35]. Isolating pEVs provides a more defined nanoscale fraction for investigating these biological activities. Previous studies have reported context-dependent effects of pEV preparations on inflammatory and tissue-associated cellular responses, supporting their investigation in regenerative applications[24,36,37].

Lipoproteins are abundant physiological plasma components that share biophysical properties with EVs and frequently co-isolate during standard separation procedures[38-40]. To address this challenge, we employed SMA pre-treatment before size-based isolation, adapting a previously reported purification method[25]. Purification reduced apolipoprotein abundance while retaining EV-associated markers and vesicular morphology. These findings support improved separation of EVs from lipoprotein-associated material and provide a basis for examining how preparation composition influences biological activity.

The functional comparisons revealed distinct responses to purified and unpurified preparations. Reduced lipoprotein abundance was associated with changes in macrophage inflammatory readouts and enhanced downstream hPDLC mineralisation. These observations complement evidence that pEV preparations contain bioactive molecules capable of modulating immune cell behaviour and highlight the importance of compositional characterisation when interpreting their biological effects[34].

Purification is associated with distinct inflammatory responses

Both pEV preparations attenuated LPS-induced inflammatory gene expression in macrophages and decreased the levels of TNF-α and IL-1β in the culture supernatants, demonstrating anti-inflammatory activity at both transcript and protein levels[41]. However, purified pEVs suppressed selected inflammatory transcripts and cytokine readouts less strongly than unpurified pEVs. One possible explanation is the depletion of HDL-associated material during purification. HDL can neutralise LPS, reduce oxidative stress, and dampen inflammatory signalling, potentially contributing to the activity of unpurified preparations[42-44]. Consistent with a contribution from lipoprotein-associated material, LDL/HDL reconstitution significantly reduced *Osm* expression, whereas other measured transcripts shifted numerically towards levels observed with unpurified pEVs. These findings support effects on selected inflammatory readouts rather than a uniform restoration of activity.

Purified pEVs nevertheless produced greater reductions in iNOS expression and increases in Arg1 fluorescence than unpurified pEVs. Increased CD206 fluorescence provided additional evidence of an M2-like macrophage marker profile. These changes were accompanied by reduced nuclear p65 localisation and lower phosphorylated p65 abundance alongside changes in total p65, consistent with attenuated NF-κB-associated signalling. Changes in lipoprotein composition offer one possible explanation, given the reported involvement of LDL and its modified forms in NF-κB activation[45-47]. The involvement of NF-κB in inflammatory regulation may help contextualise the differing responses across individual markers[48]. Overall, the effects on cytokines, phenotype-associated markers and p65 indicate that purification influences distinct aspects of macrophage activity rather than uniformly increasing inflammatory gene suppression.

Early inflammatory cues can contribute to the initiation of tissue repair and subsequent osteogenesis, highlighting the importance of the timing and extent of inflammatory activity during bone healing[44,49]. This provides a possible context for the enhanced mineralisation observed with CM from purified pEV-treated macrophages despite less pronounced suppression of selected inflammatory transcripts. The findings suggest that stronger suppression of every inflammatory readout is not necessarily associated with a greater mineralisation response. Whether the retained inflammatory activity contributes directly to this response remains a question for future mechanistic studies.

Conditioned medium from purified pEV-treated macrophages supports hPDLC mineralisation

The functional consequences of the differing macrophage responses were evident in downstream hPDLC assays. CM from purified pEV-treated macrophages increased the expression of selected osteogenesis-associated genes and significantly enhanced mineralisation. These findings are consistent with previous reports linking EV-mediated immune regulation to osteogenic differentiation[50,51]. Notably, on day 3, hPDLCs exposed to CM from purified pEV-treated macrophages showed increased expression of *ALP*, *OCN*, *BSP* and *OPN*, indicating an early transcriptional response involving matrix formation and mineralisation-associated markers[50,52,53]. In contrast, CM from unpurified pEV-treated macrophages reduced *BSP* and *OPN* expression and did not significantly enhance mineralisation relative to the control.

Differences in the composition of macrophage-derived CM may contribute to these responses. Previous studies have implicated interleukin-6 (IL-6)-associated signalling in osteogenic differentiation and communication between immune and skeletal cells[54,55]. IL-6 may also activate STAT3, promoting the transcription of matrix- and mineralisation-associated genes in other experimental models[50]. In the present study, macrophages treated with purified pEVs showed higher *Osm* expression than those treated with unpurified pEVs. However, IL-6 and oncostatin M (OSM) protein levels in CM and STAT3 activation in hPDLCs were not directly assessed, and further investigation is needed to establish the mechanisms underlying the observed osteogenic responses. Moreover, the species-specific receptor activity of mouse-derived OSM limits its interpretation as a mediator of hPDLC responses[56]. Nevertheless, hPDLCs exposed to CM from purified pEV-treated macrophages exhibited greater mineralised nodule formation on days 14 and 21 than those in the control and unpurified pEV-CM groups. Previous reports linking the osteogenic effects of macrophage-derived CM to BMP and Wnt/β-catenin signalling pathways provide potential directions for further mechanistic investigation[49,57,58].

CM from purified pEV-treated macrophages also promoted cementum-associated gene expression in hPDLCs. In particular, *CEMP1* expression was elevated on both days 3 and 7. Given the reported role of CEMP1 in cementoblast differentiation and mineral formation, this sustained transcriptional response supports its potential relevance to cementogenic differentiation[59,60]. *CAP* expression was also significantly increased on day 7. CAP has been associated with the adhesion and differentiation of periodontal ligament cells into cementoblast progenitors, suggesting a possible contribution to cementogenic responses[59]. However, the potential contribution of residual treatment-derived EVs to these responses cannot be excluded. These transcriptional changes and the enhanced mineralisation response support further investigation of CM from purified pEV-treated macrophages in periodontal tissue repair.

Study limitations

The absence of a control group receiving CM from LPS-stimulated macrophages without EV treatment limits the interpretation of the hPDLC responses. Although the findings demonstrate differences between CM from pEV-treated and purified pEV-treated macrophages, the contribution of EV treatment cannot be fully distinguished from the baseline effects of macrophage-derived CM. Future studies should include this control to clarify the contribution of EV-mediated macrophage modulation to hPDLC differentiation and

mineralisation. Furthermore, the potential presence of residual EVs in the collected CM represents another limitation. Despite thorough washing of macrophages prior to CM collection, complete removal of residual EVs could not be confirmed. Consequently, macrophage-derived EVs and potentially residual treatment-derived EVs may have contributed to the observed hPDLC responses. Further investigations incorporating EV-depletion procedures and characterisation of the resulting CM are therefore necessary to distinguish the respective contributions of soluble mediators and EV-associated components to osteogenic differentiation.

The cross-species model also warrants consideration. Mouse-derived OSM exhibits species-specific receptor activity, which limits its interpretation as a mediator of human cell responses. Studies using human macrophages and direct assessment of cytokine activity and downstream signalling would help clarify the mechanisms underlying the observed effects. In addition, the hPDLCs originated from a single donor, and validation across multiple donors would strengthen the generalisability of the findings.

Although these *in vitro* findings provide a foundation for further investigation, they do not fully reproduce the complex interactions between inflammation and tissue repair *in vivo*. Evaluation in an appropriate mouse periodontitis model, using histological and immunological analyses, is needed to determine whether the observed cellular responses translate into reduced inflammation and periodontal tissue regeneration.

Conclusion

This study supports SMA-based purification as an effective strategy for reducing lipoprotein-associated material in pEV preparations while retaining EV-associated markers and vesicular morphology. Purified pEVs exhibited a distinct immunomodulatory profile, including changes consistent with attenuated NF-κB-associated signalling. CM from purified pEV-treated macrophages enhanced hPDLC mineralisation and increased the expression of selected bone- and cementum-associated genes. Overall, these findings associate pEV purification with altered macrophage responses and enhanced differentiation-associated activity *in vitro*, supporting further investigation of purified pEVs for periodontal tissue regeneration.

DECLARATIONS

Acknowledgments

The authors acknowledge the Queensland node of the Australian National Fabrication Facility, supported by the National Collaborative Research Infrastructure Strategy, for assistance with extracellular vesicle characterisation. The authors also acknowledge Microscopy Australia (ROR: 042mm0k03) at the Centre for Microscopy and Microanalysis, The University of Queensland, supported by the National Collaborative Research Infrastructure Strategy, and thank Dr Koifman N for acquiring the cryo-TEM images. The Graphical Abstract was created with BioRender.com. (2026) https://BioRender.com/acq6cdh.

Authors' contributions

Conceptualised the study: Xu T, Zhou Y
Contributed to the study design: Xu T, Iannotta D, Tang Z, Zhou Y
Performed data collection: Xu T, Iannotta D, Tang Z, Johnson N
Performed data analysis and interpretation: Xu T, Zhou Y
Led the drafting of the manuscript: Xu T
Critically revised the manuscript for important intellectual content: Iannotta D, Tang Z, Han P, Ivanovski S, Wolfram J, Zhou Y
Supervised the study: Ivanovski S, Zhou Y
Performed the literature search: Xu T, Zhou Y

Availability of data and materials

The datasets generated and/or analysed during the current study are available from the corresponding authors upon reasonable request.

AI and AI-assisted tools statement

During the preparation of this manuscript, the AI tool ChatGPT (GPT-5, released 2025-08-07) was used to assist with English language editing and grammatical refinement. The tool did not influence the study design, data collection, analysis, interpretation, or the scientific content of the work. All authors take full responsibility for the accuracy, integrity, and final content of the manuscript.

Financial support and sponsorship

This work was supported by The University of Queensland (Wolfram J), the Australian Periodontology Research Foundation Project Grant (Xu T and Zhou Y), and the Australian and New Zealand Bone and Mineral Society (ANZBMS)-Bone Health Foundation (BHF) Grant-in-Aid (Zhou Y).

Conflicts of interest

Wolfram J currently serves or has previously served as a board member or scientific advisor for biomedical companies, including Omnidermal, Genomill, and Pharmatest Services. These companies do not specifically focus on extracellular vesicles. Ionis Pharmaceuticals, Sartorius, and Sanofi currently sponsor or have previously sponsored extracellular vesicle or nanomedicine research in the Wolfram Laboratory. Han P is a member of the Junior Editorial Board of the journal *Extracellular Vesicles and Circulating Nucleic Acids*. Han P was not involved in any steps of the editorial process for this manuscript, including reviewer selection, manuscript handling, or decision-making. The other authors declare that there are no conflicts of interest.

Ethical approval and consent to participate

This project was approved by the University of Queensland Human Research Ethics Committee (approval Nos. 2022/HE000652 and 2019/HE000134). Informed consent for the research use of donated plasma and periodontal tissue samples was obtained from the respective donors. Specifically, ethical approval No. 2022/HE000652 covered the collection of human plasma samples for the isolation and characterisation of plasma-derived extracellular vesicles (pEVs). Ethical approval No. 2019/HE000134 covered the collection of human oral tissue samples for the isolation and culture of primary human periodontal ligament cells (hPDLCs) used in subsequent in vitro experiments.

Consent for publication

Not applicable.

Copyright

© The Author(s) 2026.

Supplementary Materials

Supplementary Materials

REFERENCES

1. Van Dyke TE, Sima C. Understanding resolution of inflammation in periodontal diseases: is chronic inflammatory periodontitis a failure to resolve? *Periodontology 2000* 2020;82:205-13. DOI PubMed
2. Genco RJ, Sanz M. Clinical and public health implications of periodontal and systemic diseases: an overview. *Periodontology 2000.* 2020;83:7-13. DOI PubMed
3. Garaicoa-Pazmino C, Fretwurst T, Squarize CH, et al. Characterization of macrophage polarization in periodontal disease. *J Clin Periodontol.* 2019;46:830-9. DOI PubMed
4. Deng D, Zhang J, Gan D, et al. Roles of extracellular vesicles in periodontal homeostasis and their therapeutic potential. *J Nanobiotechnol.* 2022;20:1757. DOI PubMed PMC
5. Ivanovski S. Periodontal regeneration. *Aust Dent J.* 2009;54:S118-28. DOI PubMed
6. Zhou Y, Xiao Y. The development of extracellular vesicle-integrated biomaterials for bone regeneration. *Adv Exp Med Biol.* 2020;1250:97-108. DOI PubMed
7. Xing Y, Cheng Z, Wang R, Lv C, James TD, Yu F. Analysis of extracellular vesicles as emerging theranostic nanoplatforms. *Coord Chem Rev.* 2020;424:213506. DOI

8. Wang T, Xing Y, Cheng Z, Yu F. Analysis of single extracellular vesicles for biomedical applications with especial emphasis on cancer investigations. *TrAC Trends Anal Chem.* 2022;152:116604. DOI
9. Cai R, Wang L, Zhang W, et al. The role of extracellular vesicles in periodontitis: pathogenesis, diagnosis, and therapy. *Front Immunol* 2023;14:1151322. DOI PubMed PMC
10. van Niel G, D'angelo G, Raposo G. Shedding light on the cell biology of extracellular vesicles. *Nat Rev Mol Cell Biol.* 2018;19:213-28. DOI PubMed
11. Broad K, Walker SA, Davidovich I, Witwer K, Talmon Y, Wolfram J. Unraveling multilayered extracellular vesicles: speculation on cause. *J Extracell Vesicles.* 2023;12:e12309. DOI PubMed PMC
12. Witwer KW, Wolfram J. Extracellular vesicles versus synthetic nanoparticles for drug delivery. *Nat Rev Mater.* 2021;6:103-6. DOI PubMed PMC
13. Born LJ, Mcloughlin ST, Dutta D, et al. Sustained released of bioactive mesenchymal stromal cell-derived extracellular vesicles from 3D-printed gelatin methacrylate hydrogels. *J Biomed Mater Res A.* 2022;110:1190-8. DOI PubMed PMC
14. Kou M, Huang L, Yang J, et al. Mesenchymal stem cell-derived extracellular vesicles for immunomodulation and regeneration: a next generation therapeutic tool? *Cell Death Dis* 2022;13:5034. DOI PubMed PMC
15. Wang L, Wei X, He X, et al. Osteoinductive dental pulp stem cell-derived extracellular vesicle-loaded multifunctional hydrogel for bone regeneration. *ACS Nano.* 2024;18:8777-97. DOI PubMed
16. Zhou Y, Xu T, Wang C, Han P, Ivanovski S. Clinical usage of dental stem cells and their derived extracellular vesicles. *Prog Mol Biol Transl Sci.* 2023;199:297-326. DOI PubMed
17. Walker SA, Aguilar Díaz De león JS, Busatto S, et al. Glycan node analysis of plasma-derived extracellular vesicles. *Cells.* 2020;9:1946. DOI PubMed PMC
18. Watson JJJ, Pati S, Schreiber MA. Plasma transfusion: history, current realities, and novel improvements. *Shock.* 2016;46:468-79. DOI PubMed
19. Burnouf T, Chou M, Lundy DJ, Chuang E, Tseng C, Goubran H. Expanding applications of allogeneic platelets, platelet lysates, and platelet extracellular vesicles in cell therapy, regenerative medicine, and targeted drug delivery. *J Biomed Sci.* 2023;30:972. DOI PubMed PMC
20. Zhao X, Huang S. Plasma extracellular vesicle: a novel biomarker for neurodegenerative disease diagnosis. *Extracell Vesicles Circ Nucl Acids.* 2024;5:569-73. DOI PubMed PMC
21. Hou Y, Wen X, Zhou L, Fang X. The value of platelet-rich plasma-derived extracellular vesicles in modern medicine. *Ann Med.* 2023;55:2287705. DOI PubMed PMC
22. Lou K, Luo H, Jiang X, Feng S. Applications of emerging extracellular vesicles technologies in the treatment of inflammatory diseases. *Front Immunol.* 2024;15:1364401. DOI PubMed PMC
23. Tao X, Xue F, Xu J, Wang W. Platelet-rich plasma-derived extracellular vesicles inhibit NF-κB/NLRP3 pathway-mediated pyroptosis in intervertebral disc degeneration via the MALAT1/microRNA-217/SIRT1 axis. *Cell Signal.* 2024;117:111106. DOI PubMed
24. Adamczyk AM, Leicaj ML, Fabiano MP, et al. Extracellular vesicles from human plasma dampen inflammation and promote tissue repair functions in macrophages. *J Extracell Vesicles.* 2023;12:12331. DOI PubMed PMC
25. Iannotta D, Amruta A, Lai A, et al. Chemically-induced lipoprotein breakdown for improved extracellular vesicle purification. *Small.* 2024;20:e2307240. DOI PubMed
26. Busatto S, Yang Y, Walker SA, et al. Brain metastases-derived extracellular vesicles induce binding and aggregation of low-density lipoprotein. *J Nanobiotechnol.* 2020;18:722. DOI PubMed PMC
27. Wang X, Pham A, Kang L, et al. Effects of adipose-derived biogenic nanoparticle-associated microRNA-451a on toll-like receptor 4-induced cytokines. *Pharmaceutics.* 2022;14:16. DOI PubMed PMC
28. Walker SA, Davidovich I, Yang Y, et al. Sucrose-based cryoprotective storage of extracellular vesicles. *J Extracell Vesicles.* 2022;1:100016. DOI PubMed PMC
29. Mastronarde DN. Automated electron microscope tomography using robust prediction of specimen movements. *J Struct Biol.* 2005;152:36-51. DOI PubMed
30. Welsh JA, Goberdhan DC, O'Driscoll L, et al. Minimal information for studies of extracellular vesicles (MISEV2023): from basic to advanced approaches. *J Extracell Vesicles.* 2024;13:e12404. DOI PubMed PMC
31. Théry C, Witwer KW, Aikawa E, et al. Minimal information for studies of extracellular vesicles 2018 (MISEV2018): a position statement of the International Society for Extracellular Vesicles and update of the MISEV2014 guidelines. *J Extracell Vesicles.* 2018;7:1535750. DOI PubMed PMC
32. Kumar V, Butcher SJ, Öörni K, et al. Three-Dimensional cryoEM reconstruction of native LDL particles to 16Å resolution at physiological body temperature. *PLoS ONE.* 2011;6:e18841. DOI PubMed PMC

33. Wojczynski MK, Glasser SP, Oberman A, et al. High-fat meal effect on LDL, HDL, and VLDL particle size and number in the Genetics of Lipid-Lowering drugs and diet network (GOLDN): an interventional study. *Lipids Health Dis.* 2011;10:571. DOI PubMed PMC
34. Cheow ESH, Cheng WC, Lee CN, de Kleijn D, Sorokin V, Sze SK. Plasma-derived extracellular vesicles contain predictive biomarkers and potential therapeutic targets for myocardial ischemic (MI) injury. *Mol Cell Proteomics.* 2016;15:2628-40. DOI PubMed PMC
35. Tan Y, Kao W, Boppart M, Sweedler JV. Plasma-derived extracellular vesicle proteomics. *J Proteome Res.* 2025;24:4309-21. DOI PubMed PMC
36. Wu R, Xie Y, Peng Y, et al. Young human plasma-derived extracellular vesicles rescue and reactivate IL-1β and TNF-α treated chondrocytes. *Exp Cell Res.* 2024;437:114009. DOI PubMed
37. Arteaga-Blanco LA, Evans AE, Dixon DA. Plasma-derived extracellular vesicles and non-extracellular vesicle components from APCMin/+ mice promote pro-tumorigenic activities and activate human colonic fibroblasts via the NF-κB signaling pathway. *Cells.* 2024;13:1195. DOI PubMed PMC
38. Ramirez MI, Amorim MG, Gadelha C, et al. Technical challenges of working with extracellular vesicles. *Nanoscale.* 2018;10:881-906. DOI PubMed
39. Jia Y, Yu L, Ma T, et al. Small extracellular vesicles isolation and separation: current techniques, pending questions and clinical applications. *Theranostics.* 2022;12:6548-75. DOI PubMed PMC
40. Williams S, Fernandez-Rhodes M, Law A, Peacock B, Lewis MP, Davies OG. Comparison of extracellular vesicle isolation processes for therapeutic applications. *J Tissue Eng.* 2023;14:20417314231174609. DOI PubMed PMC
41. Hagey DW, Ojansivu M, Bostancioglu BR, et al. The cellular response to extracellular vesicles is dependent on their cell source and dose. *Sci Adv* 2023;9:eadh1168. DOI PubMed PMC
42. Linton MF, Yancey PG, Davies SS, et al. The role of lipids and lipoproteins in atherosclerosis. Endotext [Internet]. 2019. PubMed
43. Fotakis P, Kothari V, Thomas DG, et al. Anti-inflammatory effects of HDL (high-density lipoprotein) in macrophages predominate over proinflammatory effects in atherosclerotic plaques. *ATVB.* 2019;39:e253-72. DOI PubMed PMC
44. Lu LY, Loi F, Nathan K, et al. Pro-inflammatory M1 macrophages promote Osteogenesis by mesenchymal stem cells via the COX-2-prostaglandin E2 pathway. *J Orthop Res.* 2017;35:2378-85. DOI PubMed PMC
45. Yang X, Zeng J, Xie K, et al. Advanced glycation end product-modified low-density lipoprotein promotes pro-osteogenic reprogramming via RAGE/NF-κB pathway and exaggerates aortic valve calcification in hamsters. *Mol Med.* 2024;30:833. DOI PubMed PMC
46. Bing T, Shanlin X, Jisheng W, et al. Dysregulated lipid metabolism and intervertebral disc degeneration: the important role of ox-LDL/LOX-1 in endplate chondrocyte senescence and calcification. *Mol Med.* 2024;30:887. DOI PubMed PMC
47. Li Y, Shi G, Liang W, et al. Allogeneic adipose-derived mesenchymal stem cell transplantation alleviates atherosclerotic plaque by inhibiting Ox-LDL uptake, inflammatory reaction and endothelial damage in rabbits. *Cells.* 2023;12:1936. DOI PubMed PMC
48. Liu D, Zhong Z, Karin M. NF-κB: a double-edged sword controlling inflammation. *Biomedicines.* 2022;10:1250. DOI PubMed PMC
49. Huang R, Wang X, Zhou Y, Xiao Y. RANKL-induced M1 macrophages are involved in bone formation. *Bone Res.* 2017;5:BFboneres201719. DOI PubMed PMC
50. Yin X, Yang C, Wang Z, et al. Alginate/chitosan modified immunomodulatory titanium implants for promoting osteogenesis *in vitro* and *in vivo*. *Mater Sci Eng C.* 2021;124:112087. DOI PubMed
51. Cui Y, Hong S, Xia Y, et al. Melatonin engineering M2 macrophage-derived exosomes mediate endoplasmic reticulum stress and immune reprogramming for periodontitis therapy. *Adv Sci.* 2023;10:e2302029. DOI PubMed PMC
52. Vimalraj S. Alkaline phosphatase: structure, expression and its function in bone mineralization. *Gene.* 2020;754:144855. DOI PubMed
53. Chen Y, Li Z, Zhou M, et al. A comparative analysis of the osteogenic capacity of osteoblasts from newborn and two-week-old rats. *Acta Histochem.* 2022;124:151858. DOI PubMed
54. Nowwarote N, Sukarawan W, Kanjana K, Pavasant P, Fournier BPJ, Osathanon T. Interleukin 6 promotes an *in vitro* mineral deposition by stem cells isolated from human exfoliated deciduous teeth. *R Soc Open Sci.* 2018;5:180864. DOI PubMed PMC
55. Purwaningrum M, Giachelli CM, Osathanon T, Rattanapuchpong S, Sawangmake C. Dissecting specific Wnt components governing osteogenic differentiation potential by human periodontal ligament stem cells through interleukin-6. *Sci Rep.* 2023;13:35569. DOI PubMed PMC
56. Adrian-Segarra JM, Sreenivasan K, Gajawada P, Lörchner H, Braun T, Pöling J. The AB loop of oncostatin M (OSM) determines species-specific signaling in humans and mice. *J Biol Chem.* 2018;293:20181-99. DOI PubMed PMC
57. Yan C, Li N, Xiao T, et al. Extracellular vesicles from the inflammatory microenvironment regulate the osteogenic and odontogenic differentiation of periodontal ligament stem cells by miR-758-5p/LMBR1/BMP2/4 axis. *J Transl Med.* 2022;20:3412. DOI PubMed PMC
58. Tu B, Liu S, Liu G, et al. Macrophages derived from THP-1 promote the osteogenic differentiation of mesenchymal stem cells through the IL-23/IL-23R/β-catenin pathway. *Exp Cell Res.* 2015;339:81-9. DOI PubMed

59. Liu J, Zhao Z, Ruan J, et al. Stem cells in the periodontal ligament differentiated into osteogenic, fibrogenic and cementogenic lineages for the regeneration of the periodontal complex. *J Dent.* 2020;92:103259. DOI PubMed

60. Zheng X, Wang S, Xiao L, et al. LiCl -induced immunomodulatory periodontal regeneration via the activation of the Wnt/β-catenin signaling pathway. *J Periodontal Res.* 2022;57:835-48. DOI PubMed PMC

Disclaimer/Publisher's Note: All statements, opinions, and data contained in this publication are solely those of the individual author(s) and contributor(s) and do not necessarily reflect those of OAE and/or the editor(s). OAE and/or the editor(s) disclaim any responsibility for harm to persons or property resulting from the use of any ideas, methods, instructions, or products mentioned in the content.



© The Author(s) 2026. Open Access This article is licensed under a Creative Commons Attribution 4.0 International License (https://creativecommons.org/licenses/by/4.0/), which permits unrestricted use, sharing, adaptation, distribution and reproduction in any medium or format, for any purpose, even commercially, as long as you give appropriate credit to the original author(s) and the source, provide a link to the Creative Commons license, and indicate if changes were made.